The Astrophysical Journal Letters, 797:L31 (4pp), 2014 December 20 doi:10.1088/2041-8205/797/2/L31

DRAMATIC CHANGE IN JUPITER'S GREAT RED SPOT FROM SPACECRAFT OBSERVATIONS

Amy A. Simon[1], Michael H. Wong[2], John H. Rogers[3], Glenn S. Orton[4], Imke de Pater[2], Xylar Asay-Davis[5], Robert W. Carlson[4], and Philip S. Marcus[6]
[1] NASA Goddard Space Flight Center, 8800 Greenbelt Road, Code 690, Greenbelt, MD 20771, USA
[2] Astronomy Department, University of California Berkeley, Berkeley, CA 94720, USA
[3] British Astronomical Association, Burlington House, Piccadilly, London W1J 0DU, UK
[4] Jet Propulsion Laboratory, California Institute of Technology, 4800 Oak Grove Drive, Pasadena, CA 91109, USA
[5] Potsdam Institute for Climate Impact Research, Telegraphenberg A 31, 14473 Potsdam, Germany
[6] Department of Mechanical Engineering, University of California Berkeley, 6121 Etcheverry Hall, Mailstop 1740, Berkeley, CA 94720, USA
Received 2014 November 3; accepted 2014 November 21; published 2014 December 9

ABSTRACT

Jupiter's Great Red Spot (GRS) is one of its most distinct and enduring features. Since the advent of modern telescopes, keen observers have noted its appearance and documented a change in shape from very oblong to oval, confirmed in measurements from spacecraft data. It currently spans the smallest latitude and longitude size ever recorded. Here we show that this change has been accompanied by an increase in cloud/haze reflectance as sensed in methane gas absorption bands, increased absorption at wavelengths shorter than 500 nm, and increased spectral slope between 500 and 630 nm. These changes occurred between 2012 and 2014, without a significant change in internal tangential wind speeds; the decreased size results in a 3.2 day horizontal cloud circulation period, shorter than previously observed. As the GRS has narrowed in latitude, it interacts less with the jets flanking its north and south edges, perhaps allowing for less cloud mixing and longer UV irradiation of cloud and aerosol particles. Given its long life and observational record, we expect that future modeling of the GRS's changes, in concert with laboratory flow experiments, will drive our understanding of vortex evolution and stability in a confined flow field crucial for comparison with other planetary atmospheres.

Key words: planets and satellites: atmospheres – planets and satellites: dynamical evolution and stability – planets and satellites: gaseous planets

Online-only material: color figures

1. INTRODUCTION

The red edges of Jupiter's Great Red Spot (GRS) have contracted from a longitude length of ∼21° during the *Voyager* flybys in 1979 to ∼15.°5 in *Hubble* data acquired in 2012, shrinking on average 0.°19/year over the modern era. Amateur observers documented a sudden decrease in longitudinal extent in early 2014, faster than the average rate of contraction, and *Hubble Space Telescope* (*HST*) time was granted to characterize the current state of the storm. In the 2014 *Hubble* data, the red edges of the spot span about 14.°1 in longitude, a decrease of 1.°4 (1760 km) in 21 months, a rate of change 4 times greater than typical since 1979. This change has happened without any visible extrinsic causes. Continuous monitoring by amateur observers showed no anomalous events in the surrounding region that might have affected the GRS, from mid-2011 to the end of 2013 (see the British Astronomical Association, Jupiter Section: http://www.britastro.org/jupiter/section_reports.htm).

2. SPECTRAL ANALYSIS

Another notable characteristic of the 2014 images is the deep red color of the GRS, which is normally seen only during climatic cycles when the adjacent South Equatorial Belt (SEB) "fades" or whitens, such as during the Pioneer flybys in 1974 (Rogers 1995). Red colors on Jupiter are due to absorption at blue and green wavelengths, with whiter regions showing the least absorption at short wavelengths. Spectroscopy was performed using *Hubble* images from 1995 to 2014 to determine the visible-wavelength color of the darkest core of the storm, Figure 1. In this region, the reflectance spectrum (I/F) is fairly constant from 1995 to 2009 (Sanchez-Lavega et al. 2013; Simon et al. 2014). The greatest change in I/F of up to 0.08 can be seen near 410 nm when comparing data from 1996 and 2008. The data acquired in 2014, however, show that the I/F spectrum of the GRS is depressed by 0.1 to 0.15 at all wavelengths shorter than 500 nm, and by 0.05 near 630 nm. In addition, the I/F in the 890 nm methane gas absorption band has increased by ∼0.11 since 2009, using the same filter, implying the altitudes and/or the concentrations of upper tropospheric aerosols have increased (Perez-Hoyos et al. 2009). Spectra of other red regions on the planet do not show simultaneous increases in methane-band reflectivity and short-wavelength absorption, ruling out calibration issues.

In addition to the spectral change in the core of the GRS, ratio images indicate that the spectral slope from 500 to 630 nm has steepened in 2014 compared with previous dates over most of the GRS. Figure 2 shows enhanced true color and the spectral slope from 631 to 502 nm in 2014, in comparison with similar filters in 2009. There is usually some variation in spectral slope across the GRS, as seen in 2009, but it is generally very muted when compared with a nearby cyclonic barge or small regions in the North Equatorial Belt (NEB), both of which are often redder than the GRS (Sanchez-Lavega et al. 2013; Simon et al. 2014). In 2014, however, the steepest slope is observed in the GRS core, and the entire GRS collar shows more 500 nm absorption than even dark regions of the NEB.

The steeper slope from 500 to 630 nm indicates the presence of an additional absorption not normally seen within the GRS (Simon et al. 2014). Several mechanisms could be invoked, including increased UV irradiation of the color-producing compounds, but they must also explain the increased reflectance at

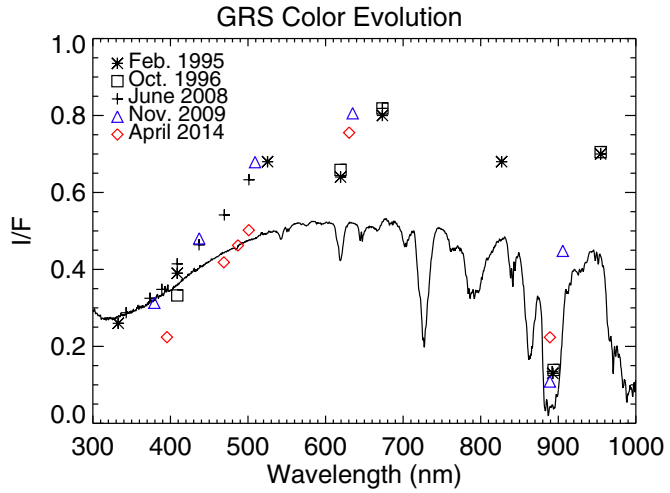

Figure 1. Spectral evolution of the core of the GRS over time from *Hubble Space Telescope* WFPC2 (1995–2008) and WFC3 (2009–2014) data. The GRS shows slight spectral variation over time, but a distinct shift is seen in the 2014 data. Solid line is a full-disk geometric albedo of Jupiter (Karkoschka 1994).

(A color version of this figure is available in the online journal.)

890 nm. The GRS changes are distinct from those observed in Oval BA in 2006, another large anticyclonic vortex, which reddened but maintained a constant 890 nm reflectivity over at least the 1995–2008 period (Wong et al. 2011). Sublimation of white ammonia ice layers mantling red cores was suggested to explain the color change of Oval BA (de Pater et al. 2010), but this mechanism is difficult to reconcile with the increased 890 nm reflectivity we observe at the GRS.

Although we do not know what compounds color Jupiter's clouds, all chromophore candidates show blue and/or green absorption, resulting in red-reflecting material. Recent laboratory work has suggested a combination of NH_3 and hydrocarbons may be photochemically processed by UV irradiation to generate a reddish material of similar spectral character to the GRS (Carlson et al. 2014). The spectral shape changes with exposure time, and longer irradiation results in depression of overall reflectance, as well as additional absorption near 500 nm. When the *Hubble* data are compared with these laboratory reflectance spectra (Figure 3), the 2014 data are show a best qualitative fit with the longest exposure time, while other dates are better fit with shorter exposures. Thus, one possible explanation for the 2014 spectrum is longer UV irradiation of aerosol particles containing NH_3 and C_2H_2, resulting in changed spectral slope and overall spectral depression, though other chromophores could also contribute (West et al. 1986). However, full chromophore comparison with laboratory work would require radiative transfer analysis to constrain the particle properties in the GRS clouds (Strycker et al. 2011); there are insufficient data from this image set to perform such modeling.

3. VELOCITY ANALYSIS

Reddening mechanisms are all tied to dynamical changes in some manner, so the determination of variation in vertical circulation or other nearby flows is critical. The internal wind speed of the GRS can top 150 m s^{-1} in a high-velocity collar that is smaller than the visual diameter of the storm (Simon-Miller et al. 2002; Asay-Davis et al. 2009; Shetty & Marcus 2010). Figure 4 shows a velocity field extracted using an automated method (AACIV; Asay-Davis et al. 2009) from the 2014 data. Correlations were calculated for box sizes of 5° in latitude/longitude, between pairs of velocity field advected images (Asay-Davis et al. 2009). The quality of the extracted velocity field was insufficient to accurately constrain the location and magnitude of the high-speed collar around the vortex due to limitations of the imaging data. Jupiter's relatively large distance from the Earth at the time of the observations resulted in 20% lower spatial resolution compared with prior *HST* analyses based on data taken near opposition. The shadow of Ganymede over the western side of the vortex in the later three frames resulted in only tie point pairs from short separations over large parts of the GRS, i.e., separations of about 43 min rather than 10 hr. The eastern area of later frames in both orbits also suffered from reduced contrast because the proximity to the limb of Jupiter resulted in a longer path length through overlying hazes and feature blurring. Within the limits of the analysis, we identify tangential velocities in the 100–150 m s^{-1} range, with higher speeds at the north–south extrema of the vortex, where it interacts with zonal jets, but with larger uncertainties than typical. Thus, preliminary manual and automated measurements of cloud motions showed no significant increase in wind speed when compared with winds measured from *Galileo*, *Cassini*, and *HST* data from 1996 to 2006 (Simon-Miller et al. 2002; Asay-Davis et al. 2009; Shetty & Marcus 2010), implying an internal circulation period of about 3.2 days for a cloud to circumnavigate the high velocity collar.

4. DISCUSSION

The GRS is centered near 22.°1 S ± 0.°2 planetographic latitude, nestled within alternating eastward and westward zonal jets. The westward jet at 19.°5 S is deflected northward around the GRS, and a broad, double-peaked, eastward jet at 26.°5 to 29° S is deflected southward, and have average wind speeds of −60 m s^{-1} and 50 m s^{-1}, respectively. These zonal wind jets can typically vary by 5–10 m s^{-1} over time and longitude depending on the cloud features present, although the 26.°5 S jet may vary by more than 20 m s^{-1} (Simon-Miller & Gierasch 2010; Asay-Davis et al. 2011). No secular change in jet speeds or locations can be correlated with the monotonically decreasing GRS area, although the temporal sampling of zonal wind fields is sparse (Simon-Miller & Gierasch 2010; Asay-Davis et al. 2011).

The latitudinal extent of the GRS has historically spanned between 10.°5 and 11°, and is currently 9.°4, the smallest size measured to date (Figure 5). There has been a slight overall trend toward latitude shrinkage of 0.°04/year, significantly slower than in the longitude dimension, but the fastest change of 0.°7 occurred between 2012 and 2014. Though the storm has a clearly diminishing length-to-width aspect ratio, from 1.8 in the *Voyager* era (and much greater historically) to 1.5 currently, the longitude and latitude spans over these dates have a correlation coefficient of 0.84.

The sudden shrinkage of the GRS and its observed color change are likely to be related to changes in zonal jet interactions. The reduction in width is due to shifts of both the northern edge (latitude mean 1979–2012, 16.°8 S ± 0.3; 2014, 17.°4 S) and the southern edge (latitude mean 1979–2012, 27.°4 S ± 0.2; 2014, 26.°8 S). This causes reduced deflection of the zonal jets north and south of the GRS, altering the zonal wind shear environment sensed by the vortex. In addition, there is decreased interaction with small vortices carried by those wind jets; eddies enter the internal flow on the GRS's eastern side, usually in the southeast quadrant. Eddies originating on the westward zonal

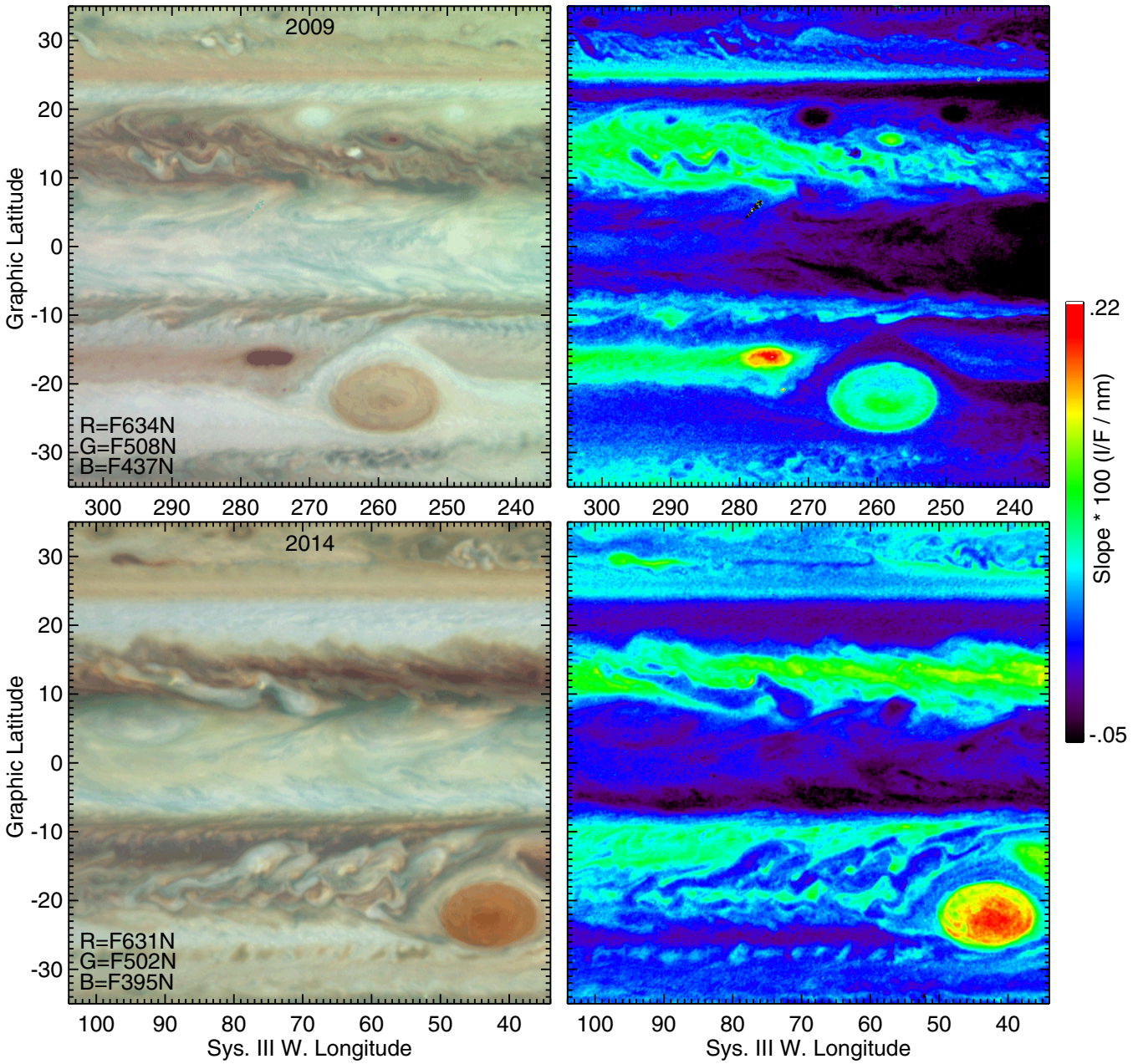

Figure 2. Comparison of the GRS and its environs from *Hubble Space Telescope* WFC3 data in 2009 and 2014. The left panels show enhanced color from 631, 502, 395 nm images in 2014 and 634, 508 and 437 in 2009 in R, G, B, respectively. The right panels show the spectral slope from ~500 to 630 nm, using those same red and green filters.

(A color version of this figure is available in the online journal.)

jet encounter the flow to the northwest of the GRS and join other eastward zonal jet eddies as they are pulled into the flow moving south of the GRS. Eddies on the northern (26.°5 S) cusp of the eastward jet can enter the flow of the GRS after passing its southern edge, while those further south pass by without interaction; this may be the reason for the altered color in 2014. In particular, in 2014 the GRS is now sufficiently withdrawn from the eastward zonal jet cusp at 26.°5 S that it does not ingest vortices carried by that zonal jet. Such small vortices often inject fresh white clouds as they enter the GRS flow and are sheared apart, as observed in movies and images captured by the *Voyager*, *Cassini*, and *Hubble* spacecraft.

A similar phenomenon occurs during SEB fading events, when there are no vortices being carried by the westward jet toward the GRS and its color intensifies (Peek 1958; Rogers 1995). In Figure 2, there is an absence in 2009 of cyclonic bright clouds northwest of the GRS in the SEB, as is typical to the start of a fading cycle (Rogers 1995). This proceeded as usual with reddening of the GRS in 2010. By 2014, the SEB showed normal activity and the GRS would have been expected to be paler; it was often quite pale in 2012, for example. Thus, the reddening of the GRS in 2014 was contrary to the usual pattern, as there was no unusual activity in the SEB to account for it.

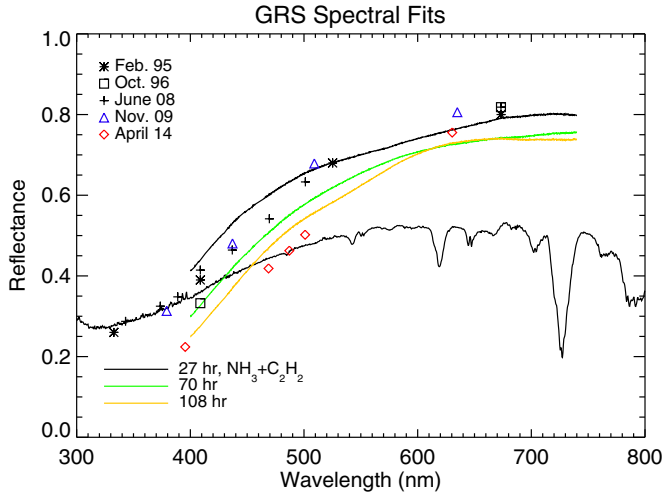

Figure 3. Qualitative fits of laboratory reflectance spectra to GRS spectra. The three laboratory data curves show ammonia and acetylene cells exposed to UV irradiation for 27, 70 and 108 hr (Carlson et al. 2014), and the resulting transmitted flux relative to the pre-irradiation spectrum.

(A color version of this figure is available in the online journal.)

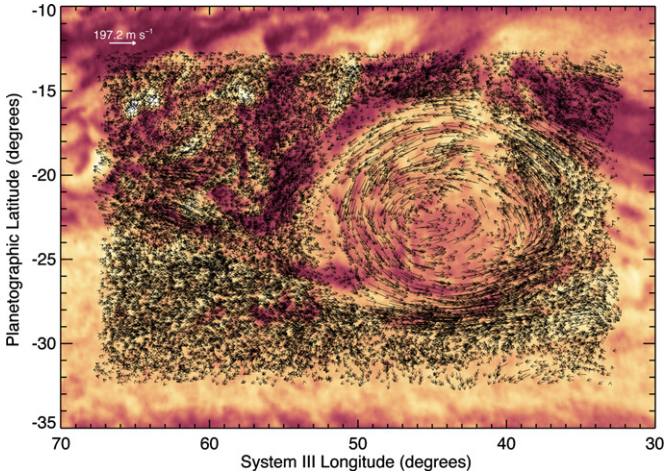

Figure 4. Velocity field of the GRS and its surroundings. Data were taken from two *HST* orbits, separated by about 10 hr, with three images per orbit. Automated extraction of correlation tie points was performed using the ACCIV method (Asay-Davis et al. 2009). Despite the apparent density of the velocity vectors, limitations in the imaging data led to large velocity uncertainties, precluding accurate quantitative comparison of the flow field to prior results.

(A color version of this figure is available in the online journal.)

5. CONCLUSIONS

It is not yet clear how large vortices such as the GRS interact energetically with the zonal wind jets. Which of these feeds energy or momentum into the other is uncertain and dependent on assumptions about the depth of the zonal wind jets. Nor is it understood what colors the clouds and why they can vary in spectral slope and absolute brightness, though the current spectrum may be indicating a change in colored-particle production. Further analyses of the temperatures, winds, and size of the GRS over time will provide interesting constraints to analytic models of geostrophic balance in the region. In addition,

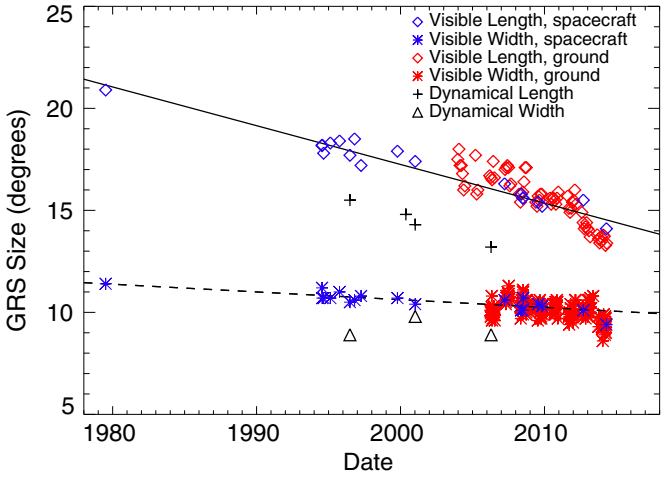

Figure 5. Change in GRS north–south and east–west size over time as measured by visible appearance and by velocity field. Visible longitude span is diminishing at a rate of $\sim 0.^{\circ}19$/year (dashed line), while visible latitude span changes at about $0.^{\circ}04$/year (solid line) on average; spacecraft data are shown in blue, amateur ground-based measurements in red. The dynamical span is determined by the location of the peaks of the internal velocities, and while smaller, show a similar trend.

(A color version of this figure is available in the online journal.)

global circulation modeling of the GRS in its flow field for different dates will show which configurations are most stable to decay.

This work was based on observations made with the NASA/ESA *Hubble Space Telescope* under programs GO12045 and GO13631. Support for these programs was provided by NASA through grants from the Space Telescope Science Institute, which is operated by the Association of Universities for Research in Astronomy, Inc., under NASA contract NAS5-26555. The changes were initially identified, and supporting data provided, by amateur observers, especially Damian Peach, and the JUPOS team, especially Michel Jacquesson.

REFERENCES

Asay-Davis, X. S., Marcus, P., Wong, M. H., & de Pater, I. 2009, Icarus, 203, 164
Asay-Davis, X. S., Marcus, P., Wong, M. H., & de Pater, I. 2011, Icarus, 211, 1215
Carlson, R. W., Baines, K. H., Anderson, M. S., et al. 2014, Icarus, submitted
de Pater, I., Wong, M. H., Marcus, P. S., et al. 2010, Icarus, 210, 742
Karkoschka, E. 1994, Icarus, 111, 174
Peek, B. M. 1958, The Planet Jupiter (London: Faber & Faber)
Perez-Hoyos, S., Sanchez-Lavega, A., Hueso, R., et al. 2009, Icarus, 203, 516
Rogers, J. H. 1995, The Giant Planet Jupiter (Cambridge: Cambridge Univ. Press)
Sanchez-Lavega, A., Legarreta, J., Garcia-Melendo, E., et al. 2013, JGRE, 118, 2537
Shetty, S., & Marcus, P. S. 2011, Icarus, 210, 182
Simon, A. A., Sanchez-Lavega, A., Legarreta, A., et al. 2014, JGRE, submitted
Simon-Miller, A. A., & Gierasch, P. J. 2010, Icarus, 210, 258
Simon-Miller, A. A., Gierasch, P. J., Beebe, R. F., et al. 2002, Icarus, 158, 249
Strycker, P. D., Chanover, N. J., Simon-Miller, A. A., et al. 2011, Icarus, 215, 552
West, R. A., Strobel, D., & Tomasko, M. 1986, Icarus, 65, 161
Wong, M. H., de Pater, I., Asay-Davis, X. S., et al. 2011, Icarus, 215, 211